

FEDSM2013-16108

**EXPERIMENTAL METHODS FOR INVESTIGATING THE DISCRETE DROPLET
IMPACT PHENOMENA OF A MODEL FLUID RELEVANT FOR LNG HEAT
EXCHANGERS**

Amy L. Brunsvold and Åsmund Ervik

SINTEF Energy Research
Sem Sælands vei 11, NO-7465
Trondheim, Norway

He Zhao

Norwegian University of Science and Technology
(NTNU)
Kolbjørn Hejes vei 1B, NO-7491
Trondheim, Norway

ABSTRACT

To improve knowledge on the design and operational issues of heat exchangers used in the liquefaction process of liquefied natural gas (LNG), experiments were conducted to investigate the complex two-phase flow phenomena in an n -pentane environment. Special focus was placed on characterizing the impact thresholds (bouncing, coalescence, splashing, etc.) of n -pentane droplets impinging on a flowing liquid film of various angles. In the phase diagram of velocity and diameter, the threshold of splashing for n -pentane was found to be below that for water (i.e. lower translational energies lead to splashing). The splashing threshold was well-characterized by a model reported previously for water droplets on stationary surfaces, adjusted slightly for non-normal impacts, which is influenced greatly by the thickness of the liquid film. In addition, the bouncing threshold of n -pentane was found to decrease with higher liquid film velocities with a threshold generally lower than that of water.

NOMENCLATURE

Symbols

D	Droplet diameter
E_T	Droplet translational energy
H	Film Height
L	Film length
LNG	Liquefied Natural Gas
m	droplet mass
Oh	Droplet Ohnesorge number

Q	Liquid flow rate
Re_f	Film Reynolds number
V	Droplet Velocity
V_m	Mean film velocity
W	Film width
We_c	Critical droplet Weber number
$We_{c,n}$	Normal, Critical Weber number

Greek symbols

Δ	film thickness
Δ^*	dimensionless thickness
θ	impact angle
μ	liquid viscosity
ρ	liquid density
σ	surface tension
φ	$90^\circ - \theta$

INTRODUCTION

Droplet impact phenomena have been the focus of many studies in recent years due to their wide applications in different fields [1-5]. The results have aided in the design and development of gas-liquid separation units, such as scrubbers, and heat exchangers [6-8]. Many industrial processes involve the interactions between droplets and liquid films. A representative example can be found in the liquefaction process in a liquefied natural gas (LNG) plant. In order to develop an energy efficient LNG plant with low emissions, compact and efficient heat exchangers must be designed. The most efficient heat transfer occurs when the working fluid and the walls of the heat

exchangers are in contact and the fraction of splashing droplets in the gas phase are limited to maximize the heat transfer. It is a challenge to accurately estimate and design the equipment without an understanding of the phenomena. Typical engineering tools in use today need to be improved to be more accurate and more robust for designing and optimizing efficient LNG heat exchangers. Without an improved physical understanding of these complex two-phase flows in heat exchangers, improving these tools is a difficult challenge. In such heat exchangers, the (mixed) refrigerants on the cold side form a two-phase region, where droplets are dynamically entrained from or coalesced into a moving liquid film. The model for the evolution of a liquid film, and hence the heat transfer, can be improved by studying the spectra of entrainment and coalescence of droplets.

Impingement studies of droplets on either a dry or a liquid-covered surface has been investigated over the past hundred years, and the understanding of the phenomena has been improved remarkably during the last two decades [5, 9]. In the literature there are two major focuses; the characterization of different impact flow regimes and the study of the impact process evolutions. It has been found that most of the research considered droplets impinging on a non-moving target, while only a few [10-12] studied nearly normal impingement of droplets on a moving target. Water has been the most common liquid for studying these phenomena [13-17] and many general models have been proposed.

Farrall *et al.* [18] developed a model for considering droplet-moving film interactions for modeling a bearing chamber. The droplet-film model considers the impact of the droplet with the film in terms of the splashing parameter. If the droplet does not splash the impact is further classified into the regimes of stick, rebound, and spread. However the model is based on droplet-wall experiments following the work of Mundo *et al.* [15], that characterized the deposition and splashing phenomena for droplet impacting on a dry wall, with a threshold supported by the model from Farrall. A more appropriate limit between deposition and splashing has been suggested to be Eq. 1, correlating the Weber number and the dimensionless film number, which was suggested by Cossali *et al.* [13] for the normal impact of droplets with a wetted wall. The droplet Ohnesorge number is defined as $Oh = \frac{\mu}{\sqrt{\rho\sigma D}}$ and the dimensionless thickness (Δ^*) is the ratio of the film thickness (Δ) to the droplet diameter (D). The work from Jayaratne & Mason [19] is considered as one of the first references studying oblique impact of droplets into a quiescent liquid surface. They studied the interaction of water droplets with a radii range of 0.060-0.120 mm with a clean water/air interface. This work discusses a model of a drop rebounding from a plane water surface which is considered as a simple harmonic and undamped surface. The model is capable of predicting the depth of the crater, the restoring force and the contact time. Some of the most recent work in the area is from Okawa *et al.* [20], who studied the production of secondary drops during the oblique impact of a single water drop into a quiescent water liquid surface. The work focused on determining number, mean diameter and total mass of secondary drops. The droplets diameters in the experiment were between 0.15 and 1.21 mm with an impact Weber number ranging from 7.2 to 818. The

height of the moving film was between 2 and 10 mm with impact angles in the 11° to 75° range normal to the film. An important observation from this work is that some secondary drops produced during the oblique impact are comparable to the primary drop size. Bird *et al.* [21] studied the impact of droplets on angled dry surfaces and showed that the tangential velocity can enhance or suppress a splash.

While the studies found in the literature have contributed greatly to the field, many of the models require correction factors and/or "liquid specific" variables that make it difficult to extrapolate to other liquids using dimensionless parameters alone. Therefore, the experiments described in this study focus on liquid droplets relevant for LNG heat exchangers impinging on a flowing liquid film with varying impingement angles. A model fluid for a mixed refrigerant is 80 mol% *n*-pentane and 20 mol% isooctane, but due to temperature gradients in the test cell as well as the general difficulties introduced when using mixed components, the experiments described here focus in on pure *n*-pentane. In order to improve the understanding of droplet impact phenomena relevant for heat exchangers we concentrate on *n*-pentane at its saturated state (at 40°C), with physical properties similar to those of refrigerants in LNG processes [22], to model the physical properties in the mixed refrigerant in the LNG process and thus improve models and tools for designing and optimizing heat exchangers for LNG.

EXPERIMENTAL METHODS

The experimental apparatus was a modified version of the experiments of droplet-pool interactions described in Zhao [7] and Zhao *et al.* [22]. For the present investigation, a liquid loop driven by an explosion-proof pump (Micropump, GB-P35/Lenze ATEX IEC 71-B14) and an aluminum board to create flowing films of various angles were included. A schematic drawing of the apparatus is shown in Figure 1. This setup consisted of three main parts: a light source, the test cell, and data acquisition. The light source was a collimated LED. In the test cell region, a needle (0.11 ID) connected to a liquid reservoir pressurized by ~0.5 bar N₂ was used to create droplets in the range of 0.1 – 1.8 mm and a flowing *n*-pentane film was generated and characterized. As the properties of *n*-pentane at 40°C are similar to those of the mixed refrigerants in LNG processes, and to ensure liquid-vapor equilibrium, the test cell was kept at 40°C with a heating circulator (Julabo, 12) and copper coils around the test cell. The test cell has four ports to measure of the pressure and temperature and is data-logged every 10 seconds. A high-speed camera (Vision Research, Phantom V9) assembled with a long-distance microscope (Infinity, 2) and a close-focus objective (Infinity, CF2) was used to capture the phenomena. The camera speed was set to 3872 frames per second (fps) with a resolution of 768×576 pixels.

Four parameters can be varied during the experiments:

- 1) *Angle of impact.* The board can be tilted to obtain the desired angle. Three angles are used: 7, 20, and 45°. The test cell must be drained and flushed with nitrogen before adjusting the impact angle.

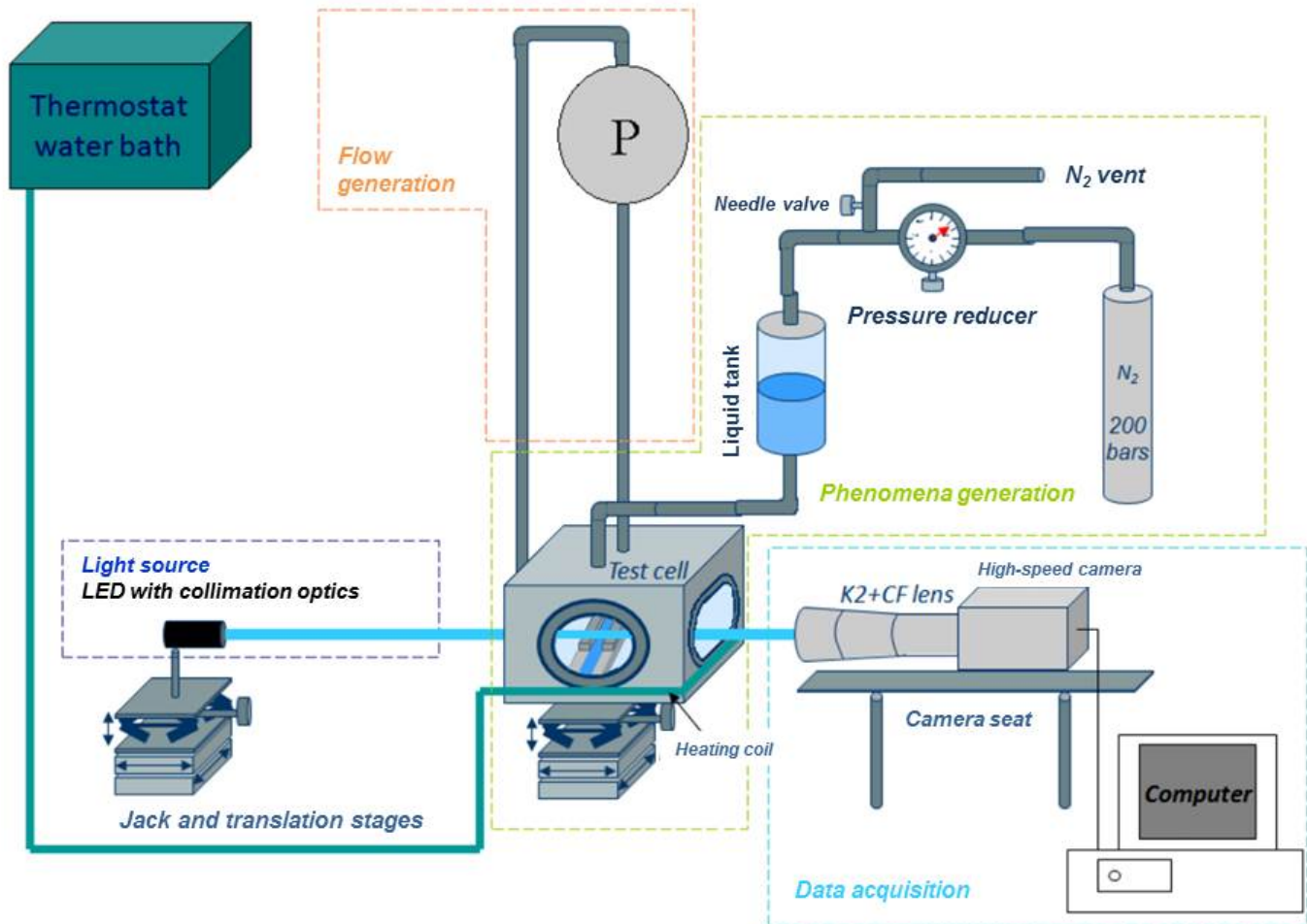


Figure 1. Schematic drawing of the experimental apparatus configured for droplet-flowing film investigations.

- 2) *Flow rate of the liquid film.* The flow rate of the liquid has been calibrated to the frequency of liquid pump. The frequencies used are 4, 6, and 8 Hz, corresponding to flow rates of 2.4, 4.0, and 6.7 $\text{m}\cdot\text{s}^{-1}$, respectively. The flow rate also affects the thickness of the fluid film.
- 3) *Velocity of the droplet.* The velocity depends on the height of the needle and the differential pressure between the liquid reservoir and the test cell. To change the position of the needle it is necessary to open the cell.
- 4) *Diameter of the droplet.* The droplet diameter can be adjusted by changing the backing pressure on the liquid tank prior to the needle. This can be done *in-situ* without opening the test cell.

For safety considerations when using a flammable liquid such as *n*-pentane, additional precautions were taken. A safety valve was used in the case of overpressure of the test cell (over 1.3 bar) and thick observation windows (~ 10 mm) were used. To prevent explosions, several measures were taken. All power supplies were current/voltage controlled, the temperature and pressure sensors used power barriers (GM International Safety, D1072D and D1914D), the heater was placed far from the test

cell, and the laboratory was adequately ventilated. All electronic equipment, including the computer, data logger, and power supplies, were out of the region where the experiments were conducted. Additionally, the test cell was partially isolated from the surrounding equipment by a Plexiglas barrier. All power sockets were placed in the middle of the wall (instead of near the floor) to prevent sparks igniting the gas, as *n*-pentane is heavier than air. Three gas detectors for hydrocarbon gasses were distributed around the laboratory

A liquid film flowing on an aluminum board ($L \times W \times H = 130 \text{ mm} \times 40 \text{ mm} \times 10 \text{ mm}$) was generated in a deep-shallow-combined channel as shown in Figure 2. Liquid *n*-pentane was delivered and injected through the top of the test cell and the liquid column formed a deep channel between a pair of metal walls on the top of the aluminum board to prevent the liquid flowing outside of the board. The shallow channel was made by of a pair of aluminum foil tape bands (3M, 425) with a thickness of about 0.1 mm to contain the developing liquid flowing film. Due to the surface tension of pentane, the flowing film thickness was raised to a higher level than the thickness of the shallow channel at the foil-edge where the film and channel-wall met. The width of the flowing film was approximately 15.5 mm, which was relatively large compared to the thickness of both the film and the channel-wall. Thus, the

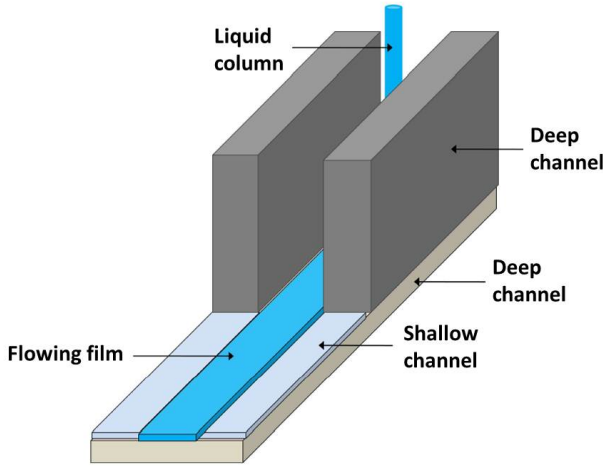


Figure 2. Schematic drawing of the component used for generating the flowing liquid film

film thickness can be considered homogeneous along the width. However, due to the entry length effect, the thickness of the flowing liquid film was not homogenous along the length. A method here is described to determine the thickness of the pentane film with a high-speed camera. The shallow channel was divided into 11 different sections for evaluating the thickness of the film. The liquid film thickness was measured by comparing an image without liquid film (i.e. dry surface) and 6 randomly-selected images with a liquid film. The measuring method applied the edge finding function in ImageJ [23] to process the images and calculate the averaged thickness using the area inside the edges. The thickness of the film did not change measurably during the droplet impacts because the frequency of the droplets was always less than 100 Hz, and often much lower.

For comparison, experiments of water impinging on a flowing water film were also conducted but are not described in detail here. Table 1(bottom) shows the density, viscosity, and surface tension of distilled water and *n*-pentane. As mentioned previously, the physical properties of *n*-pentane are similar to those of mixed refrigerants in LNG processes [22], but notably lower than those of water. The liquid film thickness was found to be lower but more independent on the flow rate than that in the experiments of water. Table 1(top) describes the various films created in which the film Reynolds number,

$$Re_f = \frac{4\rho Q}{\mu W} \quad (2)$$

with ρ liquid density, μ liquid viscosity, Q flow rate and W film width and the surface thickness, Δ , and mean velocity are listed. The mean velocity was calculated by using the flow rate, the measured film thickness, and the width of the channel. In the water experiments, the surface velocity measurement was based on tracer tracking, and the surface velocity for *n*-pentane was not measured due to the difficulties of setting tracers in a completely enclosed saturation environment.

TABLE 1. KEY PARAMETERS FOR THE FLOWING *N*-PENTANE FILMS (TOP) AND PHYSICAL PROPERTIES OF WATER AND *N*-PENTANE

Flow rate (ml/s)	3.4		5.4		7.6	
Re_f	2682		4278		6035	
Impact Angle	Δ (mm)	V_m (m/s)	Δ (mm)	V_m (m/s)	Δ (mm)	V_m (m/s)
7°	0.6	0.4	1	0.4	1.2	0.4
20°	0.5	0.5	0.7	0.5	0.7	0.7
45°	0.3	0.6	0.5	0.6	0.6	0.8

Fluid	ρ (kg/m ³)	μ (mPa·s)	σ (mN/m)
Distilled Water	996.93	0.89	71.99
<i>n</i> -pentane	605.69	0.1969	13.66

EXPERIMENTAL OBSERVATIONS

The main impact regimes found in the study of *n*-pentane droplets impinging on a flowing film with impact angles 7°, 20°, and 45° and film surface velocities ranging from 0.2 – 0.8 m s⁻¹ were found to be coalescence, bouncing, and splashing. Fewer than ~0.1% of the droplets were characterized as jetting in the entire experiment for all angles impact angles and are not analyzed or discussed here. Figure 3 illustrates a few of the phenomena observed in the *n*-pentane and water experiments. Coalescence is defined as the complete merge of an impinging droplet into a flowing liquid film without secondary droplets being generated either from the crown or as a central jet as shown Figure 3(a). Splashing is characterized by the break-up of a crown such as shown in Figure 3(b). Bouncing also occurs mainly in the velocity range from 0.6 – 0.9 m s⁻¹ and diameter range of 0.2 – 0.4 mm, with many coalescing droplets also found in this range. Figure 4 illustrates the velocity and diameter distributions of *n*-pentane droplets that were achievable in these experiments and the distribution between coalescing, splashing, and bouncing for the droplets impinging

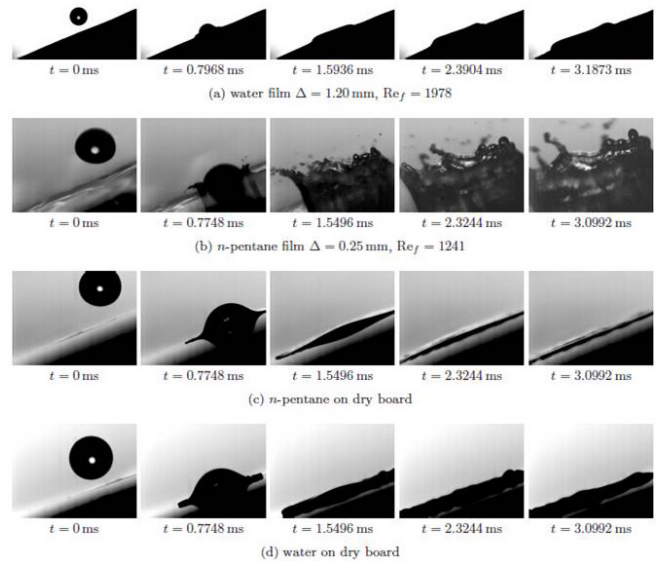


Figure 3. Water and *n*-pentane droplets with similar droplet parameters: $D = 1.7\text{--}2.0$ mm, $V = 2.0$ m s⁻¹ impinging on different targets tilted at 20°.

on 7°, 21°, and 45° tilted flowing *n*-pentane films at with thicknesses and mean flow velocities summarized in Table 1.

Coalescence can occur when the gas film at the gas-liquid surface interface breaks (due to unbalanced surface tension forces) as the droplet impinges on the surface and a capillary wave allows the droplet to join the liquid film. Splashing may occur when high-impact-energy droplets impinge on the gas/liquid film interface and a crater and strong wave are formed, leading to secondary droplets forming from the rim of the crown. In the case of bouncing droplets, the surface tension of the liquid film can absorb the kinetic energy of the droplet, much like a spring, and the restitution force will cause the drop to recoil.

Figure 3 highlights a few snapshots of water and pentane droplets with similar diameters and velocities impinging on different targets tilted at 21°. Figure 3(b) shows that the impingement of an *n*-pentane droplet causes splashing, but the impingement of water droplets at the same angle leads to non-splashing (Figure 3(a)), which can be explained to occur because of a thicker water film and higher values of surface tension and viscosity.

The comparison between Figure 3(b) and (c) shows that splashing does not occur in the absence of a flowing liquid film. These observations agree well with Vander Wal *et al.* [24] that suggested a thin film promotes splashing due to an increased kinematic gradient. Furthermore, according to [24], Sister *et al.* studied the interaction of droplets with moving films in an inclined surface with respect to the horizontal with an angle of 0°, 2°, 5°, 7°, and 10°. The work focused on studying the relationship between the size of the cavern formed by the impact of the droplet and the dependence of the total volume of secondary drops on the thickness and velocity of the liquid layer, and the slope of the tray. Alghoul *et al.* [10] studied the interaction of droplets with a horizontal moving liquid film and showed that the impact outcome regime exhibits similarities to the case of droplet-static film. Huang and Zhang [14] determined that movement of the film enhances coalescence, with the coalescence/jet formation occurring at higher values. However, the jet formation/splashing threshold is not quite affected by the film movement. In the case of the transition to splashing, the transition did not appear to be affected in the case of laminar films, and the transition mimicked the case of droplet-static film. A discussion of the various thresholds for the experiments described in this paper is described in the next section.

DISCUSSION

Coalescence-Splashing Threshold Region

A large majority of the *n*-pentane droplets investigated in these experiments coalesced, but the relative ratio of the phenomena is impossible to obtain due to the data collection method. Each droplet is individually analyzed and it is not possible to get a true cross section (i.e. the fraction of droplets for each phenomenon) of the entire process. One thing that can be assumed about the relative ratios of the phenomena is that more coalescing droplets were observed in a given time than splashing and bouncing. One of the main issues in deciphering this transition is that there is a large gap in the data from droplet diameters 0.5 – 0.9 mm and velocities 1.4 -1.7 m s⁻¹ (see Figure

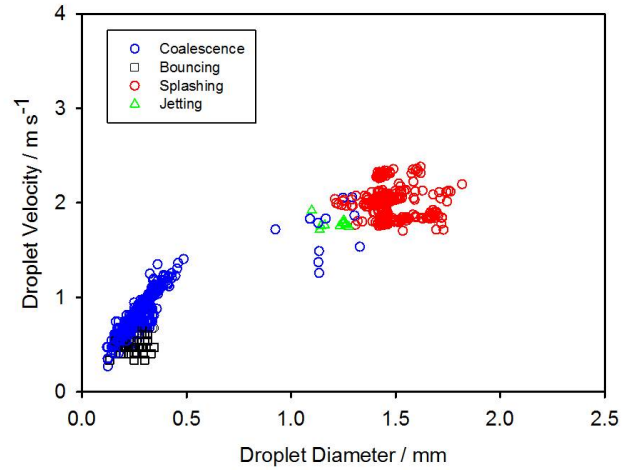


Figure 4. N-pentane droplet velocity and diameter distributions with color-coded impact phenomena.

4). Therefore it is impossible with these data to determine a coalescence – splashing threshold independently. The only impact angle where coalescing droplets were found with higher velocities and larger diameters (*i.e.* larger translational energies) was 45°. It seems more likely that the coalescence – splashing region would be similar to what was observed for 45° for all angles, but that is merely speculation. This is in agreement with an experiment conducted with water where the thresholds were primarily in the same range for all angles (internal communication). One argument against this is that there fundamentally is no difference in the method used to generate the droplets in the experiment of droplets impinging at 45°, so one could assume that the absence of droplets found in that range for 7° and 20° may be indicative of a lower threshold (lower translational energy) for these angles. However, due to the data collection method, it is also possible that these droplets were just not captured with the high-speed camera because they were out of view or focus. The few data points for jetting (around 1.2 mm and 1.8 m s⁻¹) found only for 7° impacts support this assumption. A more thorough study of this gap, whether through additional experiments or simulations, needs to be conducted. Future work is planned to use simulations from a level-set method [25] to validate these transitions. Experiments of water droplets impinging with normal impact angles have been characterized by Cossali *et al.* [13] and they present a model (Eq. 1) presented for the critical Weber number to distinguish between splashing and non-splashing events, which includes the Ohnesorge number and the dimensionless thickness, Δ^* (surface thickness, Δ / droplet diameter). As the impacts in the present investigation are on a tilted surface, the normal vector and the composite vector of the Weber number can be assumed to be determined by:

$$We_{c,n} = We \sin \varphi \quad (3)$$

where φ is equal to $90 - \theta_{\text{impact}}$. Therefore, if the motion of the liquid film is assumed to not be influential under these impacts, the normal critical Weber for the tilted boards should be roughly 0.99, 0.94, and 0.71 that of the composite critical

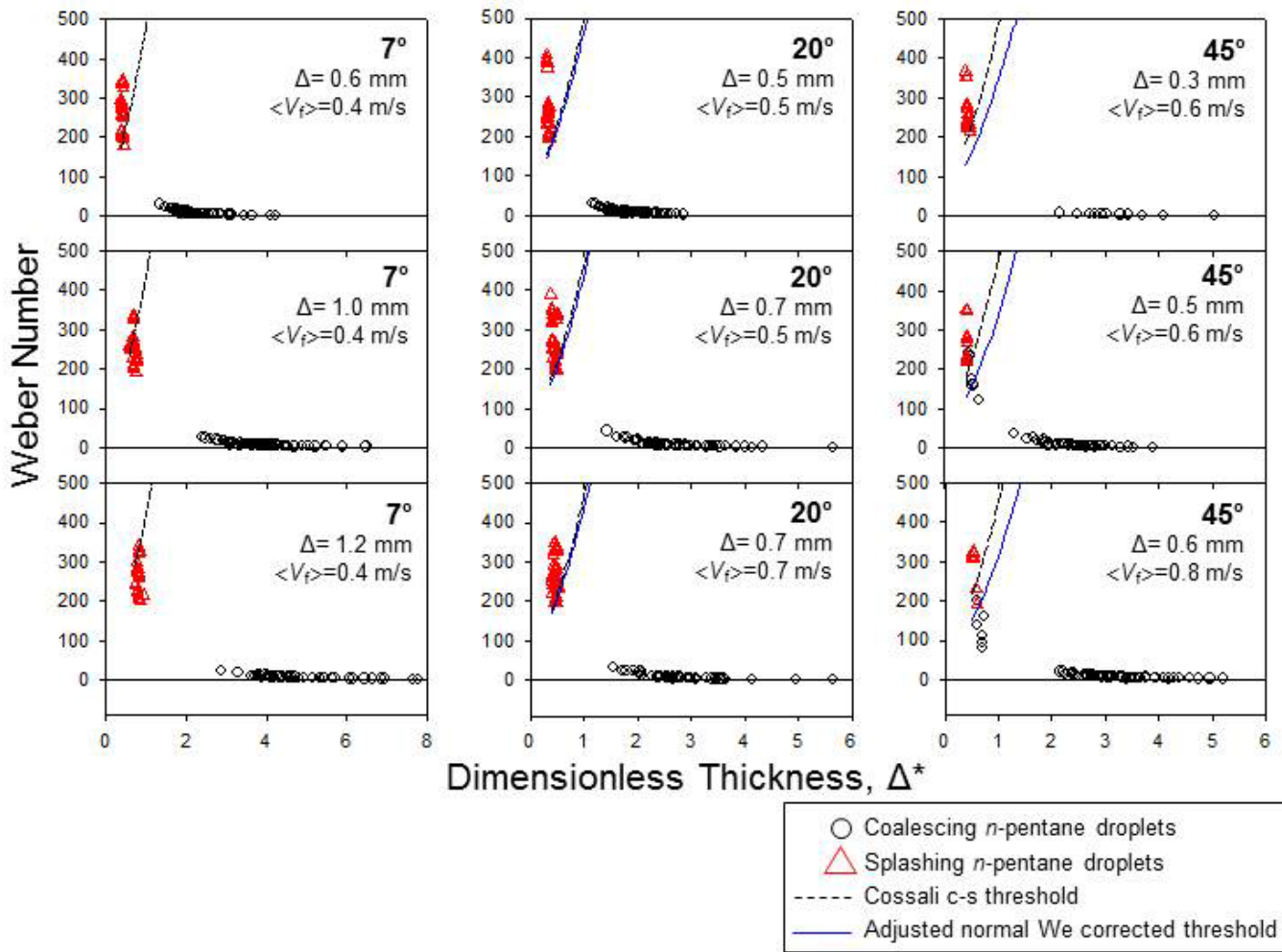


Figure 5. N-pentane droplet Weber number vector versus dimensionless thickness with comparison to the critical Weber number calculated using Eq. (1) (black-dashed line) and adjusted Weber number using the normal component of the Weber number (blue solid line).

Weber number for the 7, 20, and 45° inclined films, respectively. Figure 5 shows the Weber number versus the dimensionless thickness of the flowing films for the three film angles and corresponding film thicknesses and average film velocities. It can be seen that the Cossali threshold of splashing and non-splashing is, in general, well-characterized by Eq. (1), even without taking into account the effect of the composite Weber vector. However, if the normal Weber number is adjusted by Eq. (2), a slightly better fit to the data can be shown by the blue curves. Just as in the Cossali threshold, it appears that the agreement between the model and the experiment is better for smaller film thicknesses ($\Delta < 0.5$ mm) than for the larger thicknesses ($\Delta < 1$ mm) where the calculated threshold is overestimated. This exact trend was also shown for water droplets on inclined surfaces in an unpublished study in our group. As this trend was also seen in stationary surfaces, this verifies the assumption that the effects of the liquid film on the threshold of splashing do not play a major role, and in fact the threshold is quite similar to droplets impinging normally on a stationary film. In summary, it appears that the surface thickness is the driving factor in the droplets' thresholds, with

thicker surfaces corresponding to higher thresholds. The model could be adjusted slightly to create better fits to the experimental data for each angle and film, but this is not done here, in part because of uncertainties due to the gap in experimental data in the threshold region.

Coalescence-Bouncing Threshold Region

A representative bouncing-coalescence region is shown in Figure 6, with a droplet-surface impact angle of 20 degrees with respect to normal and showing three different surface conditions. For *n*-pentane droplets, it appears that the properties of the surface play a larger role in the droplets' translational energies needed to bounce than to coalesce. When the average surface velocity is held constant and the film thickness increases from 0.6 to 1.2 mm (e.g. 7° impact studies), there is a negligible difference in the average translational energy (i.e. corresponding diameter and velocity) of the droplets that bounce. For 7° and 20°, It is estimated that droplets with initial translational energies ($E_T = \frac{1}{2}mv^2$) around ~55 nJ may lead to bouncing. However, for 45°, the average droplet translational energy that leads to bouncing events is slightly lower, ~40 nJ.

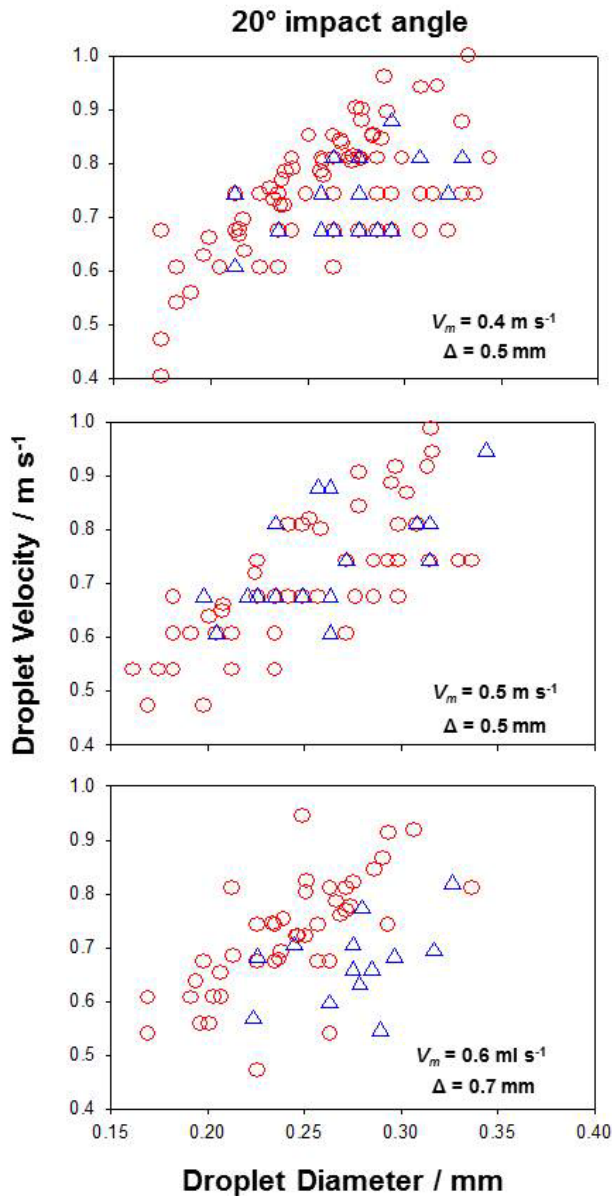


Figure 6. Bouncing (red circle) – coalescence (blue triangle) region for *n*-pentane droplets with 20 degree impact angles as a function of film thickness and velocity.

It can be seen in Figure 6 that, even in the bouncing-dominated region, a comparable number of coalescing droplets can still be found. This is due to the fact that, with the low surface tension and viscosity of *n*-pentane, the bouncing process is sensitively affected by the flowing liquid film. The flowing film introduces tangential disturbances that, on one hand, dissipate slowly due to the low viscosity. On the other hand, the intermediate layer breakup on tangential direction is promoted due to the low surface tension. For the 45° film, it can be clearly seen from the figures that the coalescence dominated-region occurs with droplet velocities greater than 0.6 m/s, which is lower than the limit ($V > 0.8 \text{ m s}^{-1}$) for the less tilted angles. This observation is contradictory to trend found in the water experiments, where, as the angle increases, the impinging energy needed for coalescence increases [26]. This again points to the fact that

coalescence is affected by the flow condition and that the flow velocity, instead of the angle, is the dominant factor for the average translational energies needed for bouncing. In the water experiments there was a low-energy coalescence region as well, but this was not found in the *n*-pentane experiments due to the difficulty in generating very low ($V < 0.3 \text{ m s}^{-1}$) droplets. Another remarkable observation is that partial coalescence phenomena is overwhelmingly suppressed in the experiments of *n*-pentane, as there are only two data points appearing in the experiments of 45° film (not shown in the figures). Investigations of Blanchette & Bigioni [27], Zhang et al. [28], Zhao et al. [29] suggested that there exists a "pinch-off" Ohnesorge number, $Oh = \text{etc.} \approx 0.023$, where D and σ are the droplet diameter and surface tension), above which partial coalescence is inhibited as the viscosity effect is dominant over the surface tension effect. By applying this pinch-off Ohnesorge number, in the experiments of water, when the Ohnesorge number was below 0.01 a large amount of partial coalescence data was present. However, the pinch-off limit does not appear to apply to the experiments of *n*-pentane, which have a comparable Ohnesorge number range of 0.001-0.003 and exhibit almost no partial coalescence. This suggests that the pinch-off limit ($Oh \approx 0.023$) may be used as a governing rule for the high-cut of partial coalescence. Meanwhile, there should be another governing limit for the low-cut, below which the inhibition of partial coalescence is reached, due to mainly the low surface tension, such as for that of *n*-pentane in this work. However, we are not trying to specifically characterize the low-cut here. It should also be mentioned that the overlap in the bouncing and coalescence region is not due to a systematic error in the experiments -the experiments conducted with water in air showed a clear transition between the two regimes and a critical Weber number could be used to determine the threshold. The high film Reynolds numbers in the *n*-pentane experiments also suggest that local disturbances in the films play a role in the droplets' tendency to bounce or coalesce and in such a film a droplet with the exact diameter and velocity could either bounce or coalesce depending on the characteristics of the film at the impact point.

LINKS TO HEAT EXCHANGER MODELING FOR THE LIQUEFACTION OF NATURAL GAS (LNG)

Detailed experiments on vertical impacts on a deep, stationary pool conducted by Zhao [7] led the way to simulating the LNG heat exchanger environment by including *n*-pentane in the portfolio of liquids studied. While these experiments aided in the understanding of the fundamental differences of the behavior of droplets with diverse physical properties, further studies were needed to illustrate how complex impact situations, including thin films with varying roughness, flowing velocities, and angles, can affect the thresholds and behavior of the interaction regimes. One interesting relationship is the impact phenomena of the droplets and heat transfer, both to the walls and the droplets in the gas phase. A crisis known as dry-out can occur when liquid entrainment, deposition, and evaporation leads to complete depletion of the liquid film with the total amount of liquid (refrigerant) in the form of droplets. When this happens, there can be two consequences; first the

heat transfer coefficient can be reduced due to a lower thermal conductivity in the gas phase and the absence of a thin liquid film, and second, liquid droplets may develop in the outlet which may require addition components in the design, such as a separator [30]. The optimal operating conditions will be determined by the trade-off between the film thickness and the total fraction of droplets in the gas phase. In general, a larger film thickness decreases the heat transfer to the wall and droplets in the gas phase contribute little to nothing in the heat transfer. Therefore, as droplets coalesce into the liquid film, the surface thickness may increase (with the level depending on the operating conditions) and the heat transfer efficiency will thus decrease. The experiments described in this paper move this field one step further and aid in identifying the regimes of splashing, bouncing, and coalescence, but even more experiments, especially those aimed at investigating droplet interactions at surfaces with complex geometries relevant for heat exchangers, are needed.

On the modeling side, the level-set method [31] has been used to simulate the two-phase flow phenomena in LNG heat exchangers. This accurate interface tracking method is coupled to the Navier-Stokes equations, and the discontinuities in e.g. the pressure across the gas-liquid interface are handled in a sharp fashion using the Ghost Fluid Method [32]. The HCR reinitialization method is used to minimize numerical volume loss [33]. The LOLEX (local level-set extraction) method is used to accurately calculate the interface curvature in the moments before impact [25]. The combination of these methods has been used to model a droplet colliding with a deep pool. However, at the present time, the simulations cannot be directly compared with the experiments described herein or in the open literature. The main limitations are that for large droplets, the thin film effects that occur before merging are very important and are not accurately modeled in the present codes because the finest grid available in a reasonable computation time is too coarse to accurately simulate the physical phenomena occurring in the experiment. The high Reynolds numbers achieved in these experiments are outside of the range for the simulations at the moment, so more work is needed to solve these issues. However, for experiments with liquid droplets impinging vertically on deep liquid pools, some results have been obtained, and an example case study is briefly described here.

A simulation was performed of a 0.18 mm diameter water droplet falling through air at 0.29 m s^{-1} and impacting a deep pool of water. Experimental results for this case due to Zhao, Brunsvold and Munkejord are found in [22]. These results indicate that a partial coalescence occurs, but the high-speed camera used was not fast enough to capture all the details of the partial coalescence process. The simulation was performed using axisymmetry. The computational domain was $0.7 \text{ mm} \times 0.7 \text{ mm}$, resolved using a 401×401 Cartesian grid. The LOLEX method was used for curvature and normal vector calculation. A comparison of the experimental and simulation results is shown in Figure 7.

The time interval between frames for the experimental and simulation results do not match, since the simulation is unable to resolve the thin air film which forms and delays merging. It is not clear that an increased grid resolution would amend this,

as the continuum approximation may not be valid for the thin air film. Nevertheless, the simulation is able to correctly predict the partial coalescence, and the simulation agrees with experiments on the size of the daughter droplet produced, to within the camera resolution. In the experiments, this daughter droplet subsequently bounces on the pool of water. The simulation is unable to predict this, again due to the thin air film formed, and shows the daughter droplet merging with the water pool instead. This comparison shows that the initial results of droplets impinging on a stationary film are promising and further work will be conducted to compare to the flowing films described in this paper.

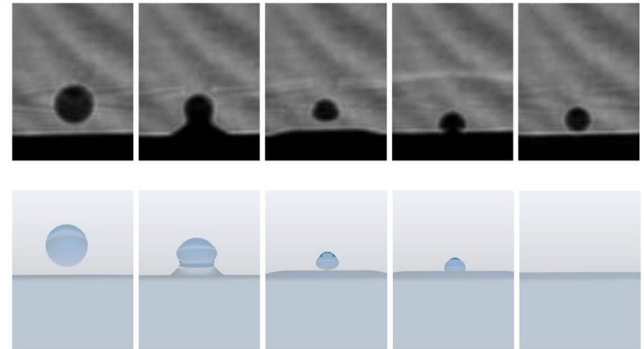


Figure 7. Experimental results (top) and simulation results (bottom) for a 0.18 mm water droplet falling through air and impacting a deep pool of water at 0.29 m s^{-1} .

CONCLUSION

This experimental study investigated *n*-pentane droplets impinging on a tilted flowing liquid *n*-pentane film. A variety of impinging conditions were achieved to include film angles of 7° , 20° , and 45° , film thickness ranging from 0.6–1.2 mm, and film velocities in the range of $0.4\text{--}0.8 \text{ m s}^{-1}$. The range of droplet diameter and velocities were 0.1–1.8 mm and $0.3\text{--}2.4 \text{ m s}^{-1}$, respectively.

The investigation shows that the threshold between coalescence and splashing can be well-characterized using a modified model suggested by Cossali et. al. [13] for normal impacts, where the only modification was to adjust the Weber number to account for non-normal impacts. From this it can be concluded that the effects from the liquid film motion on the splashing threshold are not readily exhibited but instead the film thickness is the driving factor. However, the threshold between coalescence and bouncing is difficult to quantify. The presence of a turbulent flowing film introduces disturbances which can affect the droplet phenomena. This is a clear indication that the effects from a film flow rate (and corresponding Reynolds number) are dominant on the transition of fluids with low viscosity and surface tension such as *n*-pentane. Future work to compare simulations using a modified level-set theory approach is planned.

ACKNOWLEDGMENTS

This publication is based on results from the research project *Enabling low emission LNG systems*, performed under the Petromaks program. The author(s) acknowledge the project

partners; Statoil and GDF SUEZ, and the Research Council of Norway (193062/S60) for support. The authors also acknowledge Peder Aursand and Romain Ecault for discussions and contributions in the data collection.

REFERENCES

1. Aziz, S.D. and S. Chandra, *Impact, recoil and splashing of molten metal droplets*. International Journal of Heat and Mass Transfer, 2000. **43**(16): p. 2841-2857.
2. Lander, M.J., *Nanotube arrays make droplets jump or jiggle - Structures could form hydrophobic coatings*. Photonics Spectra, 2007. **41**(9): p. 20-21.
3. Pasandideh-Fard, M., et al., *Cooling effectiveness of a water drop impinging on a hot surface*. International Journal of Heat and Fluid Flow, 2001. **22**(2): p. 201-210.
4. Tuck, C.R., M.C.B. Ellis, and P.C.H. Miller, *Techniques for measurement of droplet size and velocity distributions in agricultural sprays*. Crop Protection, 1997. **16**(7): p. 619-628.
5. Yarin, A.L., *Drop impact dynamics: Splashing, spreading, receding, bouncing...* Annual Review of Fluid Mechanics, 2006. **38**: p. 159-192.
6. Johnsen, C.G., *Experimental and numerical investigation of droplet phenomena*. 2007, Norwegian University of Science and Technology.
7. Zhao, H., *An experimental investigation of liquid droplets impinging vertically on a deep liquid pool*. 2009, Norwegian University of Science and Technology.
8. Dupuy, P.M., *Droplet deposition in high-pressure natural-gas streams*. 2010, Norwegian University of Science and Technology.
9. Pan, K.L. and C.K. Law, *Dynamics of droplet-film collision*. Journal of Fluid Mechanics, 2007. **587**: p. 1-22.
10. Alghoul, S.K., C.N. Eastwick, and D.B. Hann, *Normal droplet impact on horizontal moving films: an investigation of impact behaviour and regimes*. Experiments in Fluids, 2011. **50**(5): p. 1305-1316.
11. Sister, V., Eliseeva, O., Lednev, A., *Formation of secondary drops upon collision of a drop with a liquid surface*. Chemical and Petroleum Engineering, 2009. **45**: p. 473-477.
12. Sister, V., Eliseeva, O., Lednev, A., *Study of the features of impact reaction of a droplet with a liquid surface*. Chemical and Petroleum Engineering, 2009. **45**: p. 271-274.
13. Cossali, G.E., A. Coghe, and M. Marengo, *The impact of a single drop on a wetted solid surface*. Experiments in Fluids, 1997. **22**(6): p. 463-472.
14. Huang, Q.Y. and H. Zhang, *A study of different fluid droplets impacting on a liquid film*. Petroleum Science, 2008. **5**(1): p. 62-66.
15. Mundo, C., M. Sommerfeld, and C. Tropea, *Droplet-Wall Collisions - Experimental Studies of the Deformation and Breakup Process*. International Journal of Multiphase Flow, 1995. **21**(2): p. 151-173.
16. Shin, J. and T.A. McMahon, *The Tuning of a Splash*. Physics of Fluids a-Fluid Dynamics, 1990. **2**(8): p. 1312-1317.
17. Wang, A.B. and C.C. Chen, *Splashing impact of a single drop onto very thin liquid films*. Physics of Fluids, 2000. **12**(9): p. 2155-2158.
18. Farrall, M., et al., *A numerical model for oil film flow in an aeroengine bearing chamber and comparison to experimental data*. Journal of Engineering for Gas Turbines and Power-Transactions of the Asme, 2006. **128**(1): p. 111-117.
19. Jayaratne, O.W., Mason, B.J., *The coalescence and boundary of water drops at an air/water interface*. Proceedings of the Royal Society of London, 1964. **280**(1383): p. 545-565.
20. Okawa, T., T. Shiraishi, and T. Mori, *Effect of impingement angle on the outcome of single water drop impact onto a plane water surface*. Experiments in Fluids, 2008. **44**(2): p. 331-339.
21. Bird, J.C., S.S.H. Tsai, and H.A. Stone, *Inclined to splash: triggering and inhibiting a splash with tangential velocity*. New Journal of Physics, 2009. **11**.
22. Zhao, H., Brunsvold, A., Munkejord, S.T., Møltnvik, M., *An experimental method for studying the discrete droplet impact phenomena in a flammable gas environment*. Journal of Natural Gas Science and Engineering, 2010. **2**(5): p. 259-269.
23. Abramoff, M.D., Magelhaes, P.J., Ram, S.J., *Image processing with imagej*. Biophotonics international, 2004. **11**(7): p. 36-42.
24. Vander Wal, R.L., Gordon, W. Berger, M., Mozes, S.D., *Droplets splashing upon films of the same fluid of various depth*. Experiments in Fluids, 2006. **40**: p. 33-52.
25. Ervik, Å., *The local level-set extraction method for robust calculation of geometric quantities in the level-set method*. 2012, Norwegian University of Science and Technology.
26. Zhao, H., *An experimental investigation of water droplets impinging on a flowing liquid film of different angles*. 2011.
27. Blanchette, F. and T.P. Bigioni, *Partial coalescence of drops at liquid interfaces*. Nature Physics, 2006. **2**(4): p. 254-257.
28. Zhang, F.H., E.Q. Li, and S.T. Thoroddsen, *Satellite Formation during Coalescence of Unequal Size Drops*. Physical Review Letters, 2009. **102**(10).
29. Zhao, H., A. Brunsvold, and S.T. Munkejord, *Transition between coalescence and bouncing of droplets on a deep liquid pool*. International Journal of Multiphase Flow, 2011. **37**(9): p. 1109-1119.
30. Pacio, J.C., *Multiscale thermo-hydraulic modeling of cryogenic heat exchangers*. 2012, Norwegian University of Science and Technology.
31. Osher, S. and J.A. Sethian, *Fronts Propagating with Curvature-Dependent Speed - Algorithms Based on*

32. *Hamilton-Jacobi Formulations*. Journal of Computational Physics, 1988. **79**(1): p. 12-49.
- Liu, X.D., R.P. Fedkiw, and M.J. Kang, *A boundary condition capturing method for Poisson's equation on irregular domains*. Journal of Computational Physics, 2000. **160**(1): p. 151-178.
33. Hartmann, D., M. Meinke, and W. Schroder, *Differential equation based constrained reinitialization for level set methods*. Journal of Computational Physics, 2008. **227**(14): p. 6821-6845.